ECCD Experiments in Heliotron J, TJ-II, CHS and LHD

K. Nagasaki[a)], G. Motojima[b)], A. Fernández[c)], Á. Cappa[c)], J. M. Fontdecaba[c)], Y. Yoshimura[d)], T. Notake[d)], S. Kubo[d)], T. Shimozuma[d)], H. Igami[d)], K. Ida[d)], M. Yoshinuma[d)], T. Kobuchi[d)], Heliotron J Team[a) b)], TJ-II Team[c)], CHS Team[d)] and LHD Team[d)]

a) Institute of Advanced Energy, Kyoto University, Gokasho, Uji, Kyoto, Japan
b) Graduate School of Energy Science, Kyoto University, Gokasho, Uji, Kyoto Japan
c) Laboratorio Nacional de Fusión, EURATOM-CIEMAT, Madrid, Spain
d) National Institute for Fusion Science, Oroshi-cho, Toki, Gifu, Japan

Electron cyclotron current drive (ECCD) experiments have been made in stellarator/heliotron (S/H) devices such as Heliotron J, TJ-II, CHS and LHD. The experimental results show that ECCD can be controlled by the power injection angle, absorption position and magnetic field structure. The current drive efficiency is similar, $\gamma = n_e I_{EC} R/P_{EC}$=8-16×$10^{16}$ A/Wm^2, ζ=32.7$n_e I_{EC} R/P_W T_e$=0.03-0.05. The reversal of driven current direction is observed depending on the magnetic field ripple structure, indicating that the amplitude and direction of EC current is determined by the balance between the Fisch-Boozer effect and the Ohkawa effect, and that the Ohkawa effect is strong in S/H devices compared with tokamaks. Control of net toroidal current by using ECCD is demonstrated; net zero current state is attained by cancelling the bootstrap current.

Keywords: electron cyclotron current drive, stellarator, heliotron, Heliotron J, TJ-II, CHS, LHD, current drive efficiency, Fisch-Boozer effect, Ohkawa effect

1. Introduction

Non-inductive current has an important role on the realization of high performance plasmas and the sustainment of steady state plasmas in toroidal fusion devices. In S/H systems, no Ohmic current is required for equilibrium since the confinement magnetic field is generated by external coils. However, it is known that finite plasma pressure drives bootstrap current as well as in tokamaks, which modifies rotational transform profile, resulting that the equilibrium and stability is affected. For example, the bootstrap current increases the rotational transform in LHD, moving the rational surface of $\iota/2\pi$=1 to low shear region, giving rise to the confinement degradation due to the formation of magnetic island [1].

Electron cyclotron current drive (ECCD) is recognized as a useful scheme for stabilizing MHD instabilities and analyzing heat and particle transport [2][3]. For example, in large tokamaks such as JT-60U, neoclassical tearing mode has been stabilized by localized ECCD, leading to the improvement of normalized beta [4]. In S/H systems, on the other hand, the ECCD is expected to avoid dangerous rational surface by cancelling the bootstrap current particularly in low shear S/H devices. From the viewpoint of diagnostics, the S/H systems have the advantage of precise measurement of the EC current. The estimate of EC current is not so simple in tokamaks since a large amount of Ohmic current flows, and the effects of toroidal electric field and plasma resistivity have to be taken into account. In the S/H systems, we are able to measure the EC current with the accuracy of the order of less than 1 kA by using a conventional Rogowskii coil because of no Ohmic current.

A systematic research on ECCD in S/H systems was performed experimentally and theoretically in W7-AS for the first time [5] [6]. Several results such as the dependence on injection angle and electron density and the effect of trapped particles were discussed. Recently international collaboration research on ECCD has been conducted in Heliotron J (Kyoto Univ.) [7], TJ-II (CIEMAT) [8], CHS (NIFS) [9][10] and LHD (NIFS) [11] in order to understand the ECCD physics and to investigate the applicability of ECCD to the control of plasma equilibrium and stability. This paper summarizes these recent experimental results on ECCD. The comparison of experimental results from these four devices will give us common understanding of the current drive physics.

This paper is organized as follows. The experimental set up including the ECH/ECCD system is described in Sec. 2. The experimental results, especially the dependence on injection angle, electron density and magnetic field structure are shown in Sec. 3. The trapped

author's e-mail: nagasaki@iae.kyoto-u.ac.jp

particle effect generated by the magnetic field ripple is discussed, which strongly affects the current drive efficiency. Summary is given in Sec. 4.

2. Experimental Setup

Heliotron J, TJ-II, CHS and LHD are S/H fusion devices, which have the device parameters of major radius, R=1.2 m, minor radius, a=0.1-0.2 m, magnetic field, B=1.5 T (Heliotron J), R =1.5 m, a =0.1-0.2 m, B =1.0 T (TJ-II), R =1.0 m, a =0.2 m, B =1.9 T (CHS), and R =3.75 m, a =0.6 m, B =2.8 T (LHD). The plasma parameters discussed in this paper ranges as n_e=0.2-1.5×10^{19} m^{-3}, T_e=0.3-2 keV and T_i=0.1-2 keV. The plasmas are produced and heated by ECH only, and the upper density limit is determined by second harmonic X-mode cut-off, n_e^c = 1.75×10^{19} m^{-3} for 53.2 GHz (TJ-II and CHS), n_e^c = 3.0×10^{19} m^{-3} for 70GHz (Heliotron J), n_e^c = 4.4-×10^{19} m^{-3} for 84 GHz (LHD) and n_e^c = 17.5×10^{19} m^{-3} for 168 GHz (LHD),

The magnetic field structure is different among four devices since the field spectrum is different. Figure 1 illustrates the magnetic field profiles along the magnetic axis. Heliotron J has a capability of controlling the coil current independently, making it possible to change the magnetic ripple structure at the launching position. The magnetic field has a structure from local maximum (ripple top structure) to local minimum (ripple bottom structure) at the ECH power deposition. In TJ-II, the EC power is injected near the local minimum position. In CHS and LHD, the magnetic field ripple is small along the magnetic axis at the magnetic axis location of R=0.95 m and R=3.75 m, respectively, and the ripple structure appears when the magnetic axis is shifted by vertical coils.

The ECH/ECCD system is routinely used for plasma production and heating in S/H systems. Since the S/H system has 3-D magnetic field structure, wide injection angle range and precise polarization control are required to change the absorption profile and parallel refractive index. Recent progress on high power millimeter wave technology gives us focused Gaussian beam injection system with injection angle and polarization well controlled. Table 1 shows the main features of ECH/ECCD system in Heliotron J, TJ-II, CHS and LHD (see the references for details). The focused Gaussian beam is injected with a wide range of both toroidal and poloidal injection angle by using a steering mirror, which enables us to have enough oblique launch angle for large refractive index. In Heliotron J, a focused Gaussian beam is launched from the corner section (the toroidal angle, φ=0 deg) for $N_{||}$ scan, and non-focused Gaussian beam is launched from the straight section (φ=45 deg) for the other scans. In TJ-II, two unit 53.2 GHz ECH/ECCD

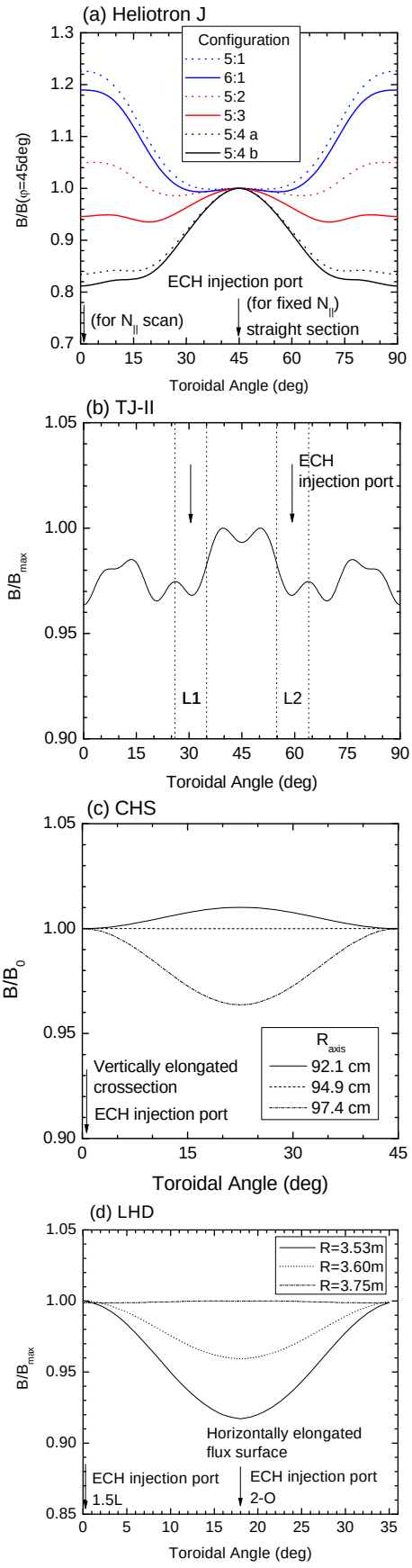

Fig. 1 Magnetic field profile along magnetic axis in (a) Heliotron J, (b) TJ-II, (c) CHS and (d) LHD.

systems are used, in which a steering mirror is installed in each injection system. The injection position is symmetric with respect to the toroidal angle, leading that the EC current can be widely controlled by scanning the injection angle with different $N_{||}$. In CHS, the EC beam is injected from the top of torus, and the refractive index is 0.16 in vacuum at the magnetic axis of R=0.95 m for the toroidal angle of 7 deg. In LHD, the toroidal angle is 8.3 deg at vertical port (1.5L port), 9.9 deg at horizontal port for co-injection, and it is -5.9 deg at vertical port, -9.9 deg for counter-injection.

	Heliotron J	TJ-II	CHS	LHD
Frequency	70GHz	53.2GHz	53.2GHz	84GHz
Maximum injection power	0.4MW	0.3MWx2	0.3MW	1.3MW
Maximum pulse length	0.2sec	0.5sec	0.1sec	3sec
Injection mode	Focused/ nonfocused Gaussian	Focused Gaussian	Focused Gaussian	Focused Gaussian
Injection angle	Controllable/ fixed	Controllable	Controllable	Controllable
Polarization	Controllable	Controllable	Controllable	Controllable
Injection mode	2nd X	2nd X	2nd X	1st O/2nd X
Reference	[12]	[13]	[14]	[15]

Table 1 Heating systems for ECCD experiment in Heliotron J, TJ-II, CHS and LHD

3. Experimental Results

Plasmas are produced and heated by the second harmonic X-mode ECH. A rough estimation of development time of total toroidal current is given by L_p/R_p where L_p and R_p are the plasma inductance and resistance. L_p/R_p is estimated from 0.1 to a few sec by assuming neoclassical conductivity. The measured toroidal current is continued to increase during discharge at low densities so that the current is somewhat underestimated in the low-density regime. Finite current may modify the rotational transform, affecting global confinement. However, neither strong confinement degradation nor MHD instabilities were observed in the experiment reported here. Details of ECCD experiment in each device are described in Refs. [7-11]

As predicted from the ECCD theory, the amplitude and driven direction depends on the parallel refractive

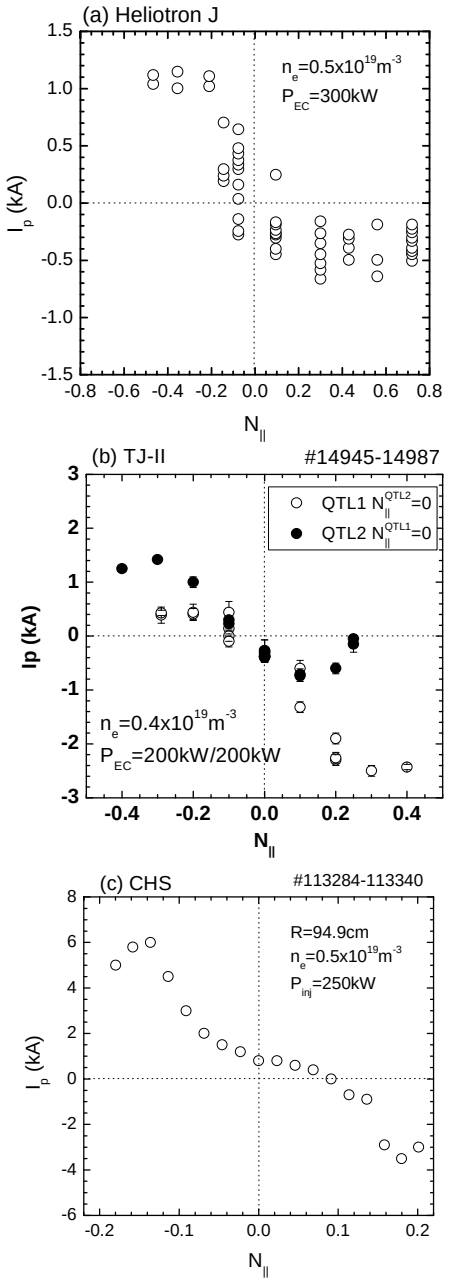

Fig.2 Dependence of toroidal current on EC injection angle. The magnetic axis in CHS is 94.9cm.

index, $N_{||}$. Figure 2 shows the dependence of the toroidal angle on the EC injection angle. It can be seen that I_p increases with increasing $N_{||}$, and saturates at a certain $N_{||}$. ECCD is a main contribution to the total current since the bootstrap current is small due to the low pressure at n_e = 0.5×10^{19} m^{-3}. The flow direction is the one expected from the Fisch-Boozer effect opposite to $\mathbf{N}_{||}$ [16]. The same tendency is observed in LHD when the injection angle is changed from the clockwise to counter-clockwise direction. The EC current amplitude is the same order, a few kA, up to now in all the devices, although the magnetic field structure is different. As discussed later, the toroidal direction of EC current strongly depends on

the magnetic ripple structure. Under the condition for toroidal injection scan, the Fisch-Boozer effect may be stronger than the Ohkawa effect. In the injection angle scan with the magnetic field fixed, the electron cyclotron resonance is Doppler-shifted due to finite $N_{||}$, resulting that the decrease in electron temperature and/or the change in ripple structure possibly affects the EC current. The $N_{||}$ dependence considering the Doppler shift effect is left for future.

The measured non-inductive current in ECH plasmas is composed of bootstrap current and EC current. The exclusion of bootstrap current is required for accurate estimation of the EC current. One method is to estimate the bootstrap current by EC beam launch in the direction normal to the magnetic field where the bootstrap current should be dominant. Another way is to use their different dependence on the magnetic field direction. The bootstrap current, which is proportional to $\mathbf{B}\times\nabla B$ drift, changes the flowing direction when reversing the magnetic field, while that of the EC current associated with the B strength does not change its flowing direction. Magnetic field reversal experiments have been conducted in Heliotron J in order to separate the EC current from the bootstrap current. We confirmed that the global plasma parameters such as stored energy and Te did not change when reversing the magnetic field direction. Figure 3 shows the density dependence of estimated bootstrap current and EC current in Heliotron J. The bootstrap current increases with increasing plasma density, and saturate at $n_e > 1.0\times10^{19}$ m^{-3}. This amplitude of bootstrap current agrees with a neoclassical prediction [17]. The bootstrap current is less than 0.5 kA at low density, which is smaller than the EC current, so that the toroidal current is mainly driven by ECCD.

In Heliotron J, the magnetic field ripple structure at power deposition position can be widely changed by controlling current in each coil. As illustrated in Fig. 1, the power deposition varies from the ripple top to the ripple bottom mainly by changing the bumpiness component in field spectrum with the magnetic field strength fixed. Figure 4 shows the density dependence of EC current for three field configurations. Here the contribution of bootstrap current is eliminated by the field reversal experiment. The maximum EC current of 4.6 kA is attained at the ripple top heating (the ratio of the magnetic field at the straight section to that at the corner section, h=1.06). The EC current flows in the opposite direction at the ripple bottom heating (h=0.82), and its amplitude is one-third as low as the ripple top heating.

One reason for current reversal is that velocity space effects are responsible for the ECCD. The Fisch-Boozer effect considers the perpendicular excursion in the velocity of a group of electrons with positive $v_{||}$.

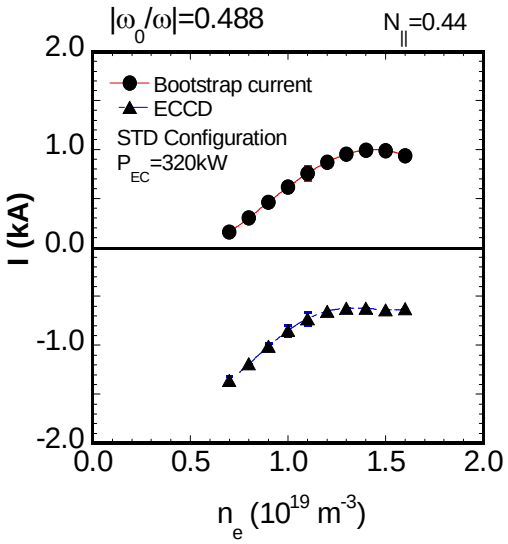

Fig.3 Separation of bootstrap current and EC current in Heliotron J.

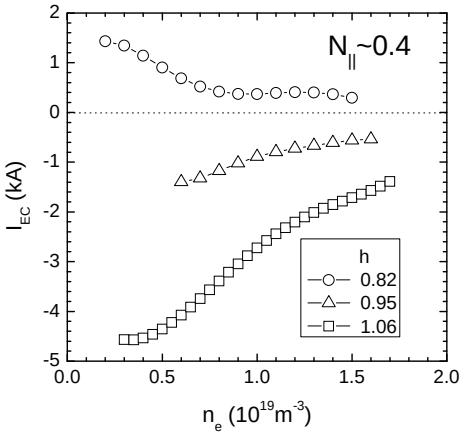

Fig.4 Density dependence of EC current in Heliotron J. The circle, triangle and square symbols denote the EC current at the ripple bottom (h=0.82), flat (h=0.95) and ripple top (h=1.06) heating, respectively.

Acceleration of these electrons causes an excess of electrons with counter-clockwise $v_{||}$, resulting in a current in the clockwise toroidal direction. On the other hand, the Ohkawa effect drives current in the opposite direction to the Fisch-Boozer current [18]. Asymmetry in $v_{||}$ is lost due to the bounce in the magnetic ripple, and a deficit in velocity space generates an electrical current in the counter-clockwise toroidal direction. In the high bumpiness configuration, the electrons are accelerated in the valley of the ripple, and they tend to become trapped, thus enhancing the Ohkawa effect. These qualitative predictions are consistent with the experimentally measured ECCD direction. The transition from the Fisch-Boozer current drive to the Ohkawa current has been demonstrated also in Ref. [5]. These suggest that the Ohkawa effect has comparable strength to the Fisch-Boozer effect in S/H systems, and the ECCD

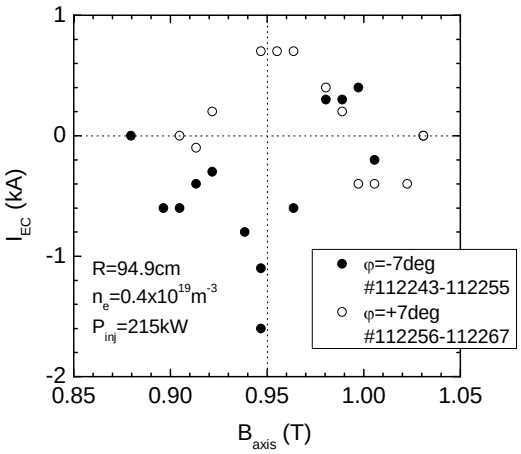

Fig.5 EC current as a function of magnetic field strength in CHS

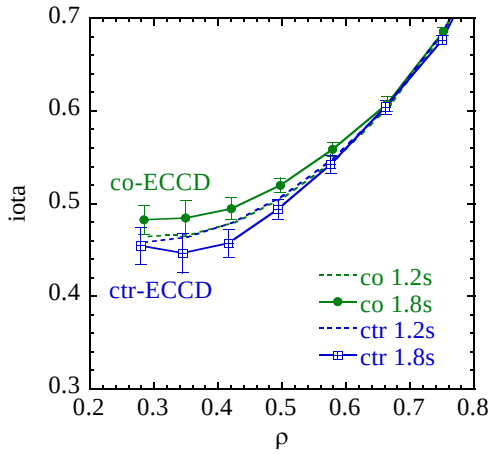

Fig. 6 Measurement of rotational transform by MSE diagnostic in LHD.

direction is determined by the difference between them.

The experimental results on magnetic field scan in CHS are shown in Fig. 5. The injection angle is +7 deg and -7 deg, and the magnetic axis is fixed; R_{axis}＝94.9 cm. The Doppler shift of cyclotron resonance is estimated as $(\omega-2\omega_{ce})/\omega \sim 1$ % for T_e=1 keV and $N_{||}$=0.16, meaning that the Doppler shift effect is weak. The EC current is largest when the resonance is located at magnetic axis. The flowing direction is consistent with the Fisch-Boozer effect. The reduction in current drive efficiency at off-axis ECCD is observed also in Heliotron J. This may be because the electron temperature is decreased and/or the ripple effect is large.

In low shear devices, even a small amount of current strongly affects rotational transform profile. According to HINT2 code simulation results on a Heliotron J configuration, a localized current of -5 kA changes the central rotational transform from 0.56 to 0.18, generating high magnetic shear at the core region. The rotational transform profile has been measured by an MSE diagnostic in LHD. Figure 6 shows the measurement results for co-ECCD, no ECCD and ctr-ECCD. The co-ECCD increases the central rotational transform, vice versa. This tendency qualitatively agrees with the direction of poloidal magnetic field generated by the measured EC current. The quantitative comparison with measured current will be done in the future experiment.

The ratio of driven current to injection power, I_{EC}/P_{EC}, and the figure of merit,

$$\gamma = \frac{n_e I_{EC} R}{P_{EC}} \qquad (1)$$

are conventionally used for the estimation of ECCD efficiency. The drawback of these functions is that they have dimension, and they do not reflect the *T*e dependence. A figure of merit describing dimensionless ECCD efficiency including the *T*e dependence is proposed in the following form [3]

$$\varsigma = \frac{e^3}{\varepsilon_0^2}\frac{n_e I_{EC} R}{P_{EC} T_e} = 32.7\frac{n_e I_{EC} R}{P_{EC} T_e} \qquad (2)$$

where parameters have a unit of n_e in 10^{20} m^{-3}, I_{EC} in A, R in m, P_{EC} in W, and T_e in keV. This dimensionless figure of merit includes important parameters such as n_e and T_e. If ζ changes under the same plasma conditions, it means that ζ reflects the effect of electron thermal velocity and trapping. Table 2 summarizes the ECCD efficiency on Heliotron J, TJ-II and CHS. No result from LHD is included since it is not estimated yet due to short ECH pulse length compared to the current evolution time. It should be noted that these efficiencies are typical values ever obtained, not optimized ones. Although the magnetic field structure is different among the devices, the EC current amount is a few kA in all the devices, and the ECCD efficiency is similar within a factor of 2. Rather low efficiency compared to tokamaks may be due to the strong Ohkawa effect enhanced by the magnetic ripple. The ray tracing calculation code is under development, which would clarify the role of trapped electrons by comparing between experiment and theory.

	Heliotron J	TJ-II	CHS
Maximum I_{EC}	4.6 kA	2 kA	6 kA
$\eta=I_{EC}/P_{EC}$	14 A/kW	10-15 A/kW	35 A/kW
$\gamma=n_e I_{EC} R/P_{EC}$	~ 8x10^{16} A/Wm^2	~ 9x10^{16} A/Wm^2	~16x10^{16} A/Wm^2
$\zeta=32.7 n_{20} I_A R_m / P_W T_{keV}$	~0.05	~0.03	~0.04

Table 2 ECCD efficiency in Heliotron J, TJ-II and CHS.

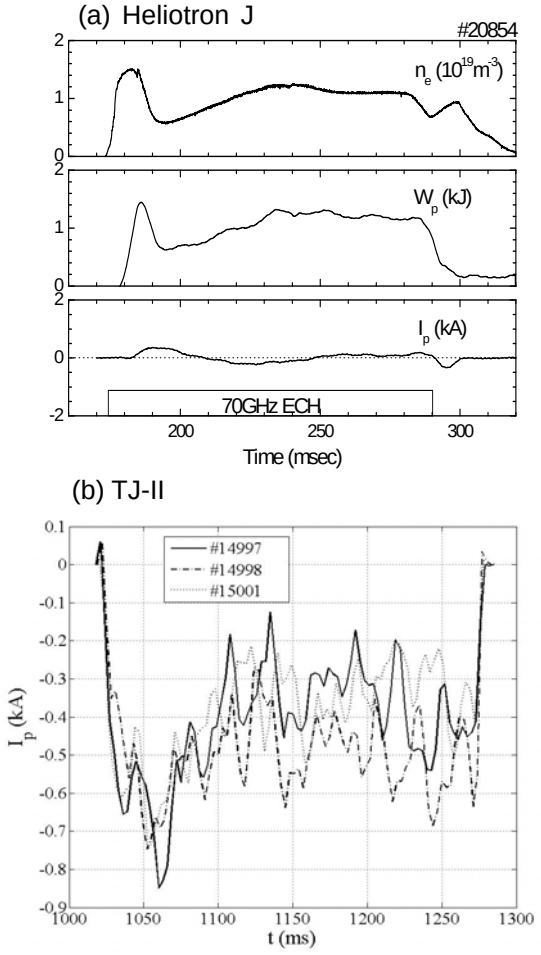

Fig.7 Demonstration of control of toroidal current, (a) zero toroidal current state in Heliotron J, (b) cancellation of EC current using two unit ECH systems in TJ-II

While the ECCD efficiency is not so high, the EC current is comparable to the bootstrap current, meaning that we are able to control the total toroidal current. Zero net current state has been demonstrated in Heliotron J as shown in Fig. 7. The total current is suppressed below 0.4 kA during the discharge by compensating the bootstrap current of 1.5 kA with ECCD. Such a state has also been demonstrated in CHS. In TJ-II, the EC current driven by each launcher is cancelled and the low current of I_{BS}=-0.5 kA is kept. The multi ECCD systems are useful for extending the current control range.

4. Conclusion

The ECCD experiment has been performed in Heliotron J, TJ-II, CHS and LHD. The driven current is affected by plasma and field parameters such as $N_{\|}$, collisionality, resonance position and magnetic field structure. The injection angle scan experiment indicates that the control ability for EC current is high. The estimated driven current and its efficiency are similar. The maximum current ever observed is 6 kA, and the ECCD efficiency is $\gamma=n_e I_{EC} R/P_{EC}$=8-16×$10^{16}$ A/Wm^2, $\zeta=32.7 n_e I_{EC} R/P_{EC} T_e$=0.03-0.05. In S/H systems, the magnetic ripple structure strongly affects the ECCD. The direction of EC current is reversed in Heliotron J when the power is deposited at the ripple bottom position, indicating that the electron trapping is a key factor to determine the EC current.

The EC current is comparable to the bootstrap current, and the ECCD has a potential to control the rotational transform profiles. The control of net current has been successfully demonstrated by compensating the bootstrap current with the EC current. Since the bootstrap current profile should be different from the EC current profile, we will need to extend the controllability of rotational transform profile connected to the suppression of MHD instabilities.

Acknowledgements

The authors are grateful to the Heliotron J, TJ-II, CHS and LHD staff for conducting the experiments. This work was partly supported by NIFS/NINS under the NIFS Collaborative Research Program (NIFS04KUHL005) and under a project sponsored by the Formation of International Network for Scientific Collaborations.

References

[1] Y. Narushima, J. Plasma and Fusion Research **1**, 004 (2006)
[2] V. Erckmann and U. Gasparino, Plasma Phys. Control. Fusion **36**, 1869 (1994),
[3] R. Prater, Phys. Plasmas **11**, 2349 (2004)
[4] K. Nagasaki, et al., 45 Nucl. Fusion **45**, 1608 (2005)
[5] V. Erckmann, et al., Fusion Eng. Design **53**, 365 (2001)
[6] H. Maaßberg, et al., Plasma Phys. Control. Fusion 47 (2005) 1137-1163
[7] G. Motojima, et al., Nucl. Fusion **47**, 1045 (2007)
[8] A. Fernández, et al., to be published in Fus. Sci. Technol.
[9] Y. Yoshimura et al., Journal of the Korean Physical Society, Vol. 49, December 2006, pp. S197-S200
[10] Y. Yoshimura, et al., to be published in Fusion Sci. Technol.
[11] T. Notake, et al., this workshop
[12] H. Shidara, et al., Fusion Sci. Technol. 45 (2004) 41
[13] A. Fernández, et al., Int. J. Infrared adn Millimeter Waves 22 (2001) 649
[14] Y. Yoshimura et al., J. Phys. Soc. Jpn., Vol.75, (2006) 114501
[15] T. Shimozuma et al. Fusio Sci Tech. **50**, 403 (2006)
[16] N. J. Fisch and A. Boozer, Phys. Rev. Lett. 45 (1980) 720
[17] G. Motojima, et al., Fusion Sci. Technol. **51**, 122 (2007)
[18] T. Ohkawa, General Atomics Report GA-A13847 (1976)